Biosensors and Bioelectronics 252 (2024) 116142

Contents lists available at ScienceDirect

Biosensors and Bioelectronics

journal homepage: www.elsevier.com/locate/bios

Capacitive immunosensing at gold nanoparticle-decorated reduced graphene oxide electrodes fabricated by one-step laser nanostructuration

Danilo Echeverri [a,c,1], Enric Calucho [a,b,1], Jose Marrugo-Ramírez [a,b], Ruslán Álvarez-Diduk [a,*], Jahir Orozco [c,**], Arben Merkoçi [a,d,***]

[a] Nanobioelectronics & Biosensors Group, Institut Català de Nanociència i Nanotecnologia (ICN2), CSIC and the Barcelona Institute of Science and Technology (BIST), Campus UAB, Bellaterra, 08193, Barcelona, Spain
[b] Universitat Autònoma de Barcelona (UAB), Bellaterra, 08193, Barcelona, Spain
[c] Max Planck Tandem Group in Nanobioengineering, Institute of Chemistry, Faculty of Natural and Exact Sciences, University of Antioquia, Complejo Ruta N, Calle 67 N° 52–20, 050010, Medellín, Colombia
[d] ICREA Institució Catalana de Recerca i Estudis Avançats, Passeig de Lluís Companys, 23, 08010, Barcelona, Spain

ARTICLE INFO

Keywords:
Capacitive nanobiosensor
Laser-reduced graphene oxide
Nanostructured electrode

ABSTRACT

Nanostructured electrochemical biosensors have ushered in a new era of diagnostic precision, offering enhanced sensitivity and specificity for clinical biomarker detection. Among them, capacitive biosensing enables ultra-sensitive label-free detection of multiple molecular targets. However, the complexity and cost associated with conventional fabrication methods of nanostructured platforms hinder the widespread adoption of these devices. This study introduces a capacitive biosensor that leverages laser-engraved reduced graphene oxide (rGO) electrodes decorated with gold nanoparticles (AuNPs). The fabrication involves laser-scribed GO-Au^{3+} films, yielding rGO-AuNP electrodes, seamlessly transferred onto a PET substrate via a press-stamping methodology. These electrodes have a remarkable affinity for biomolecular recognition after being functionalized with specific bioreceptors. For example, initial studies with human IgG antibodies confirm the detection capabilities of the biosensor using electrochemical capacitance spectroscopy. Furthermore, the biosensor can quantify CA-19-9 glycoprotein, a clinical cancer biomarker. The biosensor exhibits a dynamic range from 0 to 300 U mL^{-1}, with a limit of detection of 8.9 U mL^{-1}. Rigorous testing with known concentrations of a pretreated CA-19-9 antigen from human fluids confirmed their accuracy and reliability in detecting the glycoprotein. This study signifies notable progress in capacitive biosensing for clinical biomarkers, potentially leading to more accessible and cost-effective point-of-care solutions.

1. Introduction

In modern healthcare, electrochemical nanobiosensors have emerged as a powerful solution for point-of-care (POC) diagnostics. These sophisticated devices boast the remarkable ability to detect specific molecules of interest, such as clinical biomarkers, with unparalleled sensitivity, all within a portable and user-friendly framework (Campuzano et al., 2021; Nemčeková and Labuda, 2021; Quesada-González and Merkoçi, 2018). The advantages of electrochemical nanobiosensors are manifold, including high sensitivity, specificity, and rapid response, as well as simplicity, affordability, and the potential for miniaturization (Echeverri and Orozco, 2022a; Lopes et al., 2022). These analytical devices integrate nanomaterials and bio-materials platforms, unlocking the potential to detect biomolecules and chemical analytes with remarkable accuracy and precision (Thakur and Sankar, 2022).

In this context, significant efforts have been dedicated to integrating advanced inorganic- and organic-based nanomaterials into biosensing platforms to enhance their analytical performance (Arduini et al., 2016;

* Corresponding author.
** Corresponding author.
*** Corresponding author. Nanobioelectronics & Biosensors Group, Institut Català de Nanociència i Nanotecnologia (ICN2), CSIC and the Barcelona Institute of Science and Technology (BIST), Campus UAB, Bellaterra, 08193, Barcelona, Spain.
E-mail addresses: ruslan.alvarez@icn2.cat (R. Álvarez-Diduk), grupotandem.nanobioe@udea.edu.co (J. Orozco), arben.merkoci@icn2.cat (A. Merkoçi).
[1] These authors contributed equally to this work.

https://doi.org/10.1016/j.bios.2024.116142
Received 26 December 2023; Received in revised form 1 February 2024; Accepted 18 February 2024
Available online 20 February 2024

Nemčeková and Labuda, 2021; Zhu et al., 2014). Particularly noteworthy are the unique properties of graphene and its derivatives, such as graphene oxide (GO) and reduced graphene oxide (rGO), which possess exceptional electronic, optical, and electrochemical attributes. Metal nanoparticles (NPs) have been ingeniously integrated into them to enhance these materials further, significantly increasing their surface area and active binding sites for biomolecules. This novel approach also improves mechanical strength and electron transfer efficiency (Khalil et al., 2018). As a result, graphene-based materials, especially those decorated with metal nanoparticles, have emerged as ideal candidates for developing ultrasensitive point-of-care testing devices (Prattis et al., 2021; Scroccarello et al., 2023).

The conventional methods to fabricate electrodes for electrochemical biosensors include typically technologies like screen-printing, inkjet-printing, 3D-printing, and microfabrication (Ambaye et al., 2021; Guo et al., 2010; Orozco et al., 2007). Subsequently, such electrodes are used in their bare form, modified with NPs or coated with nanocomposites to enhance their biosensing capabilities (Barsan and Brett, 2016; Cruz-Pacheco et al., 2023; Fernández-Sánchez et al., 2009; Mendoza et al., 2008). The electrode modification is done through physical adsorption, drop-casting, ink-mixing, electrodeposition, or chemical interactions (Antuña-Jiménez et al., 2020). While effective, these strategies have limitations, such as the use of reducing compounds and capping agents, lack of precise control over decoration patterns and modifier distribution, and the need for multistep procedures, leading to costly and time-consuming fabrication processes. These challenges have impeded the widespread commercial application of such devices (Scroccarello et al., 2023).

However, a promising alternative has emerged: laser-scribing technology, offering a simple, rapid, and cost-effective means of fabricating nanostructured electrodes for biosensing applications (Giacomelli et al., 2020; Lahcen et al., 2020). Using an infrared (IR) laser, researchers have successfully obtained graphene-based nanostructured electrodes through laser irradiation of polymeric substrates, such as polyimide, polyetherimide, and polysulfone. This innovative method produces graphene and graphene-metal NP nanocomposites (Li, 2020; Ye et al., 2015; You et al., 2020). Among the pioneers in this field, Merkoçi's research group demonstrated a one-step process to develop electrochemical sensors by producing an rGO film decorated with metal NPs for detecting various compounds, including caffeic acid, nitrite, and hydrogen peroxide (Scroccarello et al., 2023). Moreover, rGO-gold nanoparticle (AuNP)-based electrodes exhibited excellent conductive properties and enabled efficient biofunctionalization with diverse biomolecules (Peña-Bahamonde et al., 2018). Although other reported works have leveraged the use of graphene derivatives and AuNPs nanocomposites (Gupta et al., 2022; Liu et al., 2021; Lu et al., 2016; Song et al., 2021) our synthesis methods are more straightforward and time-efficient.

Capitalizing on the advantages of laser-reduced graphene oxide (LRGO) electrodes, the literature is witnessing a surge in applications compatible with POC testing of clinical biomarkers, thanks to their simplicity, rapidity, affordability, and the potential for large-scale production (Prattis et al., 2021). For instance, Merkoçi's research group utilized LRGO electrodes patterned and press-stamped onto polyester sheets to detect *Escherichia coli* pathogenic bacteria amperometrically (Zhao et al., 2023). Other studies reported successful implementations of laser-induced graphene (LIG) electrodes using a polyimide film (Kapton) as a carbonaceous substrate (Lahcen et al., 2020; Muzyka and Xu, 2022) to develop electrochemical immunosensors for the detection of *Salmonella enterica* (Soares et al., 2020), IgG antibodies (Barman et al., 2020), cortisol (Nah et al., 2021), carcinoembryonic antigen (CEA) (Wang et al., 2021), interleukin-6 (Chandra Barman et al., 2021), procalcitonin (Amouzadeh Tabrizi and Acedo, 2022), tumor necrosis factor-α (Luo et al., 2023), C-reactive protein (CRP) (Tu et al., 2023) and the SARS-CoV-2 virus (Torrente-Rodríguez et al., 2020). Considering that DNA nanostructures are emerging as promising materials for electrode fabrication (N. Liu et al., 2022; Zhang et al., 2023), some reports on DNA-based biosensors that utilize laser-engraved graphene electrodes have been reported for the detection of SARS-CoV-2 (Moreira et al., 2023), *Mycobacterium tuberculosis* (Tai et al., 2021), microcystin (Wang et al., 2023), insulin (J. Liu et al., 2022), human epidermal growth factor receptor 2 (Her-2) (Rauf et al., 2021a), preeclampsia specific miRNA hsa-miR-486-5p (Wan et al., 2020), and cardiac Troponin-I (cTn-I) (Rauf et al., 2021b). Notably, Prof. Bueno's research group developed an electrochemical biosensor based on single-layer graphene electrodes modified with antibodies for the ultrasensitive detection of CRP in attomolar concentrations using quantum conductance as a response variable (Lucas Garrote et al., 2022). However, they did not explore LRGO electrodes in their work. Therefore, these electrode-based immunosensors are worth exploring by quantum capacitive interrogation. The transduction mechanism of our electrochemical nanobiosensor is based on the change of electrochemical capacitance after target binding on the electrode surface. Electrochemical capacitance ($C_{\bar{\mu}}$) can be expressed as a series of its ionic or non-faradaic (C_i) and quantum or faradaic (C_q) components, as in the following equation: $\frac{1}{C_{\bar{\mu}}} = \frac{1}{C_i} + \frac{1}{C_q}$ (Garrote et al., 2020). C_i corresponds to the double-layer capacitance, while C_q is related to the occupation of available quantum states in the interface and is proportional to the electronic density of states (DOS), such as in graphene (Gutierrez et al., 2017). In the context of nanostructured interfaces, where $C_i \gg C_q$, the quantum capacitance component governs the overall electrochemical capacitance, leading to $C_{\bar{\mu}} \approx C_q$ (Garrote et al., 2020; Lucas Garrote et al., 2022). The rGO has a prominent contribution to quantum capacitance, attributed to the charging of localized and non-localized electronic states (Gutierrez et al., 2017). $C_{\bar{\mu}}$ can be used for signal transduction in biosensors because the electronic density-of-states are susceptible to the dielectric environment modified by the receptor-molecular target biorecognition events occurring at the electrode/electrolyte interface (Lucas Garrote et al., 2022). Hence, the nanostructured interface and the proper electrochemical transduction technique in synergy enable the ultrasensitive detection of multiple biomarkers (Bueno, 2019).

Quantum capacitance is determined by impedance-derived electrochemical capacitance spectroscopy (ECS), a relatively new transduction technique introduced approximately ten years ago (Fernandes et al., 2013). The significance of impedance and impedance-derived capacitance, unlike other electrochemical techniques such as voltammetry and amperometry, lies in its ability to discriminate among all the electrical, electrochemical, and physical processes occurring at the electrode/electrolyte interface, each exhibiting different time constants (Bueno and Davis, 2014; Lazanas and Prodromidis, 2023). As with voltammetric and amperometric techniques, analyzing certain processes becomes challenging when operating in the time domain. Conversely, in the frequency domain, spanning a wide range of frequencies, impedimetric techniques simplify complex electrochemical systems by deconvoluting them into individual processes with distinct time constants, thus facilitating the analysis (Lazanas and Prodromidis, 2023).

This work presents the first capacitive immunosensor that utilizes rGO-AuNP electrodes fabricated by laser-scribing (Scheme 1A). The electrodes were carefully functionalized with an anti-human IgG antibody, enabling the detection of IgG antibodies from human serum, thus confirming the capacitive biosensing approach. Based on this differential response of the biosensor, wherein the electrochemical capacitance changes are target concentration-dependent, we successfully assembled an immunosensor for detecting the CA-19-9 glycoprotein, a critical cancer biomarker, showcasing the practical applicability of rGO-AuNP electrodes for glycoprotein-based biomarker detection (Scheme 1B). These nanostructured interfaces have tremendous potential for capacitive biosensing of multiple clinical biomarkers, boasting a label-free and reagentless operation mode, positioning them as promising candidates for POC testing devices.

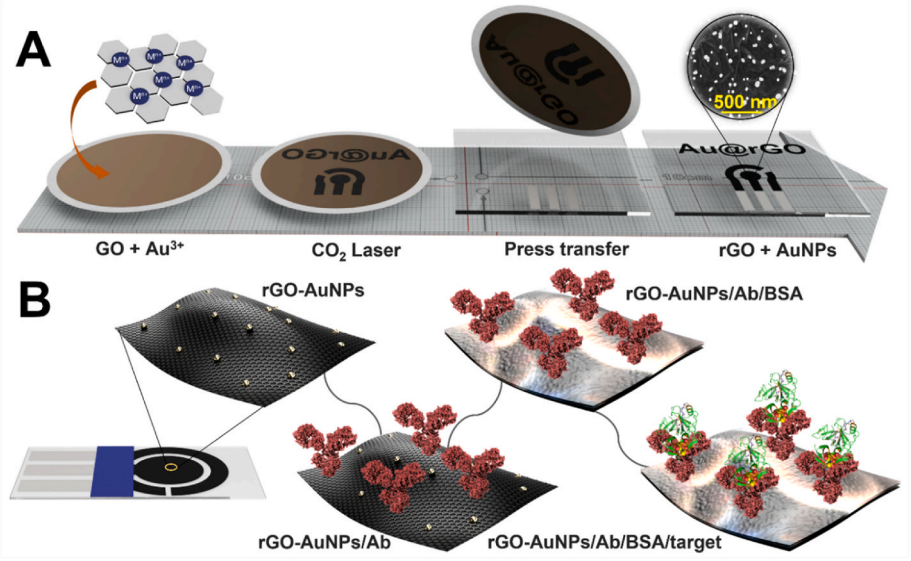

Scheme 1. A) Outline of the fabrication process of the nanostructured electrodes. GO-Au^{3+} films are irradiated with a CO_2 laser to produce rGO-AuNPs films. Parallelly, silver ink electrical connections are screen-printed onto a PET substrate. Finally, rGO-AuNPs films are aligned with the silver ink connectors and transferred. **B)** The assembly steps of the biosensing platforms are used to detect human IgG antibodies and CA-19-9 glycoprotein, respectively. First, the bioreceptor is incubated, followed by adding BSA to block the remaining free surface from non-specific interactions. Lastly, the sample containing the target molecule is incubated before electrochemical capacitance spectroscopy is performed.

2. Material and methods

The reagents and solutions, equipment, fabrication, electrochemical characterization of rGO-AuNP electrodes, and assembly of the biosensing interface are described in the supporting information (SI) section.

3. Results and discussion

3.1. Fabrication and characterization of rGO-AuNP electrodes

Scheme 1A illustrates the fabrication process of the rGO-AuNPs electrode. The fabrication of nanostructured electrodes was carefully optimized in previous work (Scroccarello et al., 2023). The GO-Au^{3+} dispersion was filtered, forming a film on polyvinylidene difluoride (PVDF), and reduced using CO_2 laser-engraving to yield the rGO-AuNPs that were transferred to the polyethylene terephthalate (PET) support. The nanostructured platform was characterized by FE-SEM and XPS. Fig. 1A shows a micrograph of the rGO-AuNPs electrode. The AuNPs were round with an average diameter of 14.4 ± 0.5 nm (Fig. 1B). The high-resolution spectrum of C1s highlights the peak with a binding energy (BE) of 284.5 eV associated with sp^2-hybridized carbon (C=C) and oxygen-containing functional groups at 285.4 and 290 eV, corresponding to hydroxyl/epoxy carbon groups (C-O) and carbonyl groups (C=O), respectively (Fig. 1C) (Scroccarello et al., 2023). For the core-level spectra of Au4f, the two sharp and asymmetric peaks recorded at 84.3 and 87.9 eV, with a spin-orbit splitting value of 3.7 eV, are characteristic of the zero-valent gold (Fig. 1D) (Scroccarello et al., 2023). The other peaks are related to the Au^{1+} gold oxidation state (BEs of 85.7 eV and 89.5 eV). The presence of Au^{1+} can be attributed to the Au coordination with GO through cation-π and electrostatic interactions (Scroccarello et al., 2023; Sylvestre et al., 2004).

The formation of rGO-AuNPs takes place as follows. The laser beam interacts with the GO film, dramatically increasing the local temperature and inducing thermal excitation of the atoms with consequent elimination of oxygen-containing groups (Li, 2020; Scroccarello et al., 2023). At the same time, the energy provided by the laser promotes the reduction of the gold cation to the metallic zero-valent state (Ghildiyal et al., 2019). In addition, GO and gold cations can interact through cation-π interaction, which favors the electron transfer process (Wang et al., 2012; Zhao and Zhu, 2020).

One notable feature of our electrodes is the easiness of preparation. The primary advantage of employing this methodology is that it reduces GO and Au^{3+} simultaneously in dry conditions, eliminating the need for inks containing solvents that might interfere with subsequent steps, such as biofunctionalization or bioassay. Since the electrode is not made of ink, no masks for screen-printing are necessary. Customized designs for the laser can be created to select the area to be engraved. Based on previous work, the rGO film thickness for this methodology was determined to be above 6 μm. The rGO surface is composed of flakes that are a few nanometers thick. Each flake measures hundreds of microns in lateral size and is approximately 20–30 nm thick (Giacomelli et al., 2020).

The presence of Au was confirmed electrochemically by the characteristic reduction peak observed by CV in H_2SO_4, which is absent on bare rGO, as shown in Fig. S1A (Kim et al., 2010; Scroccarello et al., 2023). In addition, the electrochemical characterization by CV in PBS shows a characteristic gold oxide reduction peak, as shown in Fig. 1E (Hoogvliet et al., 2000). The surface coverage of AuNPs can be calculated from the CV experiments performed in H_2SO_4. The resultant AuNPs area was estimated by using a gold surface charge of 400 μC cm^{-2} (Hou et al., 2021). The AuNPs area was 6 ± 0.5 mm^2, representing 35% of the total electroactive area. In this sense, rGO contributed to the electrode area to a greater extent. The electron transfer capability of the rGO-AuNP electrodes was assessed using the ferro/ferricyanide redox probe, as described in section 4 of Supporting Information. These experiments confirmed the conductive properties and enhanced electron transfer of rGO-AuNP electrodes (Figs. S1B–C and Tables S1–2). The electron transfer occurs directly via direct electron tunneling between the redox species and the electrode (Hui et al., 2016). A quasi-reversible behavior was obtained, and a decrease in the peak-to-peak separation (ΔE) was observed from rGO ($\Delta E = 173 \pm 6$ mV) to the rGO-AuNPs ($\Delta E = 163 \pm 6$ mV). Furthermore, the anodic/cathodic peak intensity ratio is close to one, indicating electron transfer reversibility (Elgrishi et al., 2018). As previously reported in the literature, we confirm that rGO exhibits quantum capacitance (Iamprasertkun and Dryfe, 2019; Lopes et al., 2021; Lucas Garrote et al., 2022) by the shape of the Nyquist capacitive plot, where pseudocapacitive materials form a semicircle, as

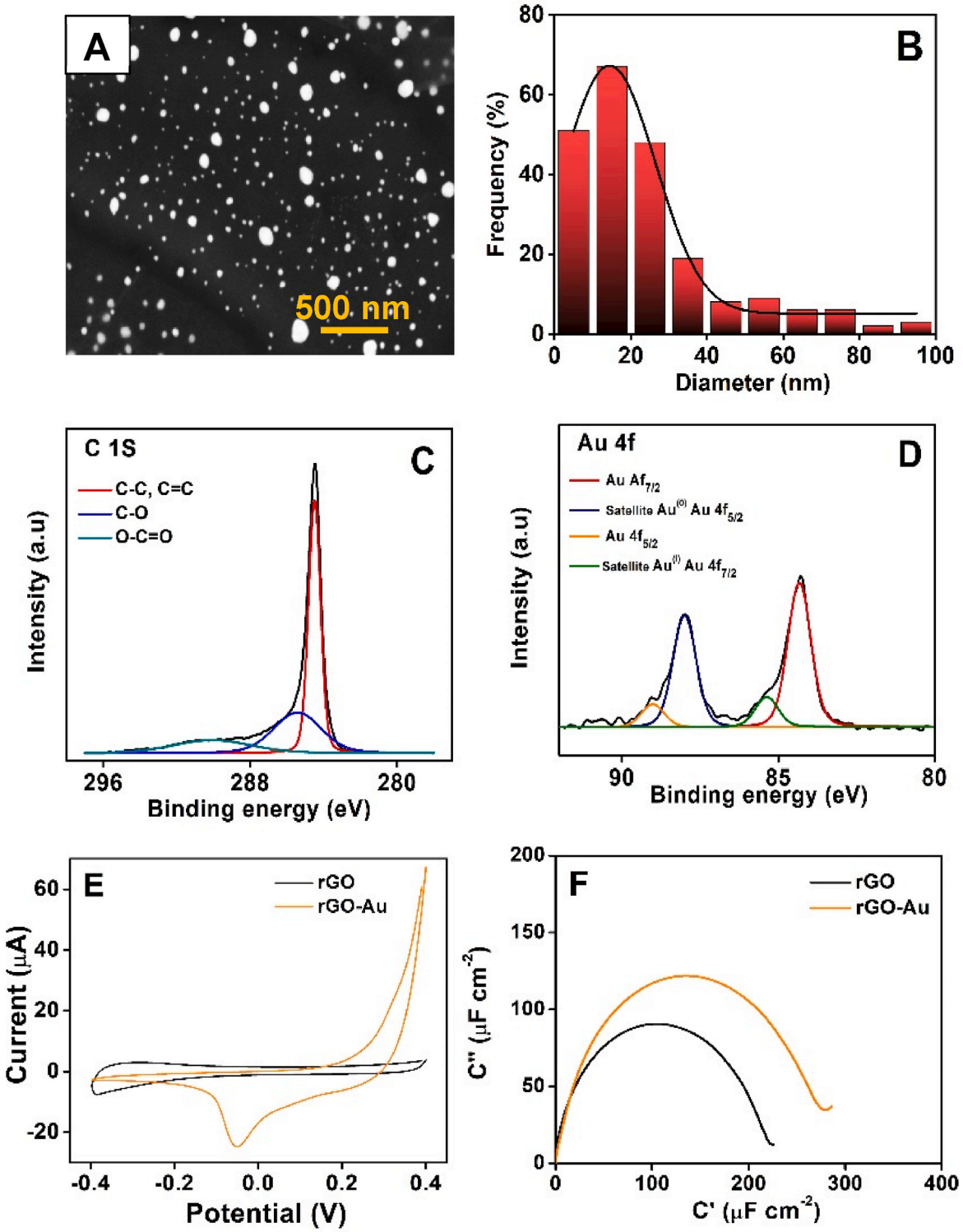

Fig. 1. **A**) FE-SEM micrograph of rGO-AuNPs electrode. **B**) Size distribution of AuNPs. **C-D**) XPS spectra of the rGO-AuNPs electrode formed with the laser treatment; core level spectra of C1s and Au4f, respectively. Electrochemical characterization of the rGO-AuNPs electrodes. **E**) Cyclic voltammograms in 50 mM PBS/0.1 M KCl pH 6.0, scan rate 100 mV s^{-1}. The black line corresponds to the rGO electrode, and the yellow line is the rGO with AuNPs. **F**) Capacitive Nyquist plots in 50 mM PBS/0.1 M KCl pH 6.0, 10 mV amplitude sinusoidal perturbation, frequency range from 100 kHz to 0.1 Hz.

shown in Fig. 1F (Allison and Andreas, 2019; Marques et al., 2015). $C_{\bar{\mu}}$ was calculated as the diameter of the semicircle of the Nyquist capacitive plot. rGO exhibited a relatively higher electrochemical capacitance ($C_{\bar{\mu}} = 214 \pm 1$ μF cm^{-2}), with respect to the $C_{\bar{\mu}}$ values reported for single-layer graphene electrodes (Lopes et al., 2021), as it has been widely reported that graphene is a two-dimensional nanomaterial with quantum capacitance (Iamprasertkun and Dryfe, 2019; Xia et al., 2009; Zhan et al., 2015). In this platform, the rGO has the maximum electronic density of states (DOS) and, therefore, the maximum electrochemical capacitance associated with localized and non-localized electronic states in the conjugated π-orbital system of the molecular structure (Gutierrez et al., 2017). Embedding AuNPs on rGO increased the $C_{\bar{\mu}}$ value to 265 ±

6 μF cm^{-2}, attributed to the AuNPs acting as electron pathways to facilitate electron transport between graphene sheets and toward the current collector (Zhang et al., 2021). The rGO-AuNPs electrode is a mesoscopic interface comprising layers of atoms with nanometer-thick sheets where accessible DOS are confined to the nanometer scale, responsive to the dielectric environment (Bueno and Davis, 2020). Thus, the quantized energy $E \propto 1/C_{\bar{\mu}}$ of a mesoscopic interface can be directly used as a transducer signal of molecular recognition events (Bueno and Davis, 2020; Lucas Garrote et al., 2022).

3.2. Biosensing interface assembly and characterization

Once the transducing signal of electrochemical capacitance from the nanostructured electrodes was established, we analyzed the specific biosensor response to the protein target. As a proof of concept, the rGO-AuNP electrodes were initially functionalized with an anti-IgG antibody to assess the performance of the nanostructured interface in biosensing. Subsequently, they were functionalized with anti-CA-19-9 antibodies to explore the practical applicability (Scheme 1B). In both cases, the rGO-AuNP electrodes were biofunctionalized with anti-IgG and anti-CA-19-9 antibodies, thereby serving as biosensing interfaces for IgG antibodies and CA-19-9 glycoprotein. The immobilization of antibodies onto the nanostructured interface was achieved through physical adsorption, driven by Van der Waals' interactions, hydrophobic effects, electrostatic forces, solvation, and hydrogen bonding (Liu and Peng, 2017; Sotnikov et al., 2019). Antibodies may attach to AuNPs through Au-S bonding, specifically with the thiol groups of exposed cysteine residues. This mechanism contributes to the stable conjugation of antibodies to AuNPs, as demonstrated in several studies (Ruiz et al., 2019; Siriwardana et al., 2013; Wang et al., 2014). Additionally, the rGO interacted with the antibodies through electrostatic, π-π stacking, and hydrophobic interactions, owing to graphene's characteristic sp^2 carbon structure (Huang et al., 2019).

Physical adsorption is a straightforward and cost-effective method compared to other immobilization techniques. It enables the direct attachment of antibodies to a surface without requiring complex chemical reactions or additional reagents. Unlike some covalent immobilization methods, physical adsorption often eliminates the need for extensive chemical modification of antibodies (Steen Redeker et al., 2013), simplifying the biosensor assembly process and reducing the risk of altering antibody properties during immobilization. Furthermore, the covalent coupling of immunoglobulins is also a random process as they have similar functional groups equally distributed in their structure. Yet, a site-directed antibody immobilization approach could be implemented to improve antibody orientation (Gao et al., 2022). Despite the disadvantages of physical adsorption, physically adsorbing antibodies is generally rapid and stable enough over gold nanostructures, allowing for quick and efficient sensor preparation, which is advantageous when time is critical, such as in POC diagnostics. Physical adsorption of antibodies on the rGO-AuNP electrodes, besides being more straightforward and faster than covalent attachment (which requires chemical activation of the surface), preserves the activity and stability of the antibodies (Peña-Bahamonde et al., 2018).

Following the adsorption of antibodies onto the nanostructured interface, a blocking step with BSA was employed to prevent non-specific protein adsorption onto the electrode surface. The immobilized antibodies on the nanostructured surface acted as bioreceptors, specifically interacting with the IgG antibody and CA-19-9 glycoprotein. The detection of these antibody-glycoprotein molecular biorecognition events relied on monitoring alterations in interfacial electrical properties at the nanostructured surface. For this purpose, variations in the $C_{\bar{\mu}}$, were monitored, corresponding to changes in the electronic DOS at the rGO-AuNPs interface linked to the biorecognition event. Hence, $C_{\bar{\mu}}$ was harnessed as a quantifiable transducer signal for detecting both IgG antibodies and CA-19-9 glycoprotein (Lucas Garrote et al., 2022; Oliveira et al., 2019).

We monitored the formation of biosensing interfaces interacting with IgG and CA-19-9 glycoproteins by tracking variations in $C_{\bar{\mu}}$ from EIS measurements at each step of the interface modification process, as previously reported (Lucas Garrote et al., 2022). The changes in $1/C_{\bar{\mu}}$ were quantified by the percentage of relative variation of the electrochemical capacitance signal, such as $RR\,(\%) = [(1/C_{\bar{\mu}(Target)} - 1/C_{\bar{\mu}\,(BSA)})/1/C_{\bar{\mu}\,(BSA)}]\,x\,100$, where $1/C_{\bar{\mu}(Target)}$ is the value of the inverse of electrochemical capacitance after the incubation with the IgG antibody or CA-19-9 glycoprotein, respectively, and $1/C_{\bar{\mu}\,(BSA)}$ is the value of the inverse of electrochemical capacitance before the sample incubation. The highest $C_{\bar{\mu}}$ value (Figs. 2A and 3A) corresponded to the rGO-AuNPs interface, where electronic DOS reached its maximum. After antibody adsorption onto rGO-AuNPs surface, the $C_{\bar{\mu}}$ decreased down to ~244 ± 0.16 and ~253 ± 18 μF cm^{-2} for the anti-IgG and anti-CA-19-9, respectively, attributed to the perturbation of DOS of rGO-AuNPs nanostructured interface (Lucas Garrote et al., 2022; Marques et al., 2015).

Upon BSA addition, $C_{\bar{\mu}}$ further decreased to ~223 ± 1 and ~234 ± 6 μF cm^{-2} for the anti-IgG and anti-CA-19-9, confirming the successful blocking of non-specific adsorption sites on the rGO-AuNPs surface. This consistent reduction in $C_{\bar{\mu}}$ after each modification step validated the physical adsorption of biomolecules onto the rGO-AuNPs surface. Subsequent evaluation of biosensor response to varying IgG concentrations confirmed the concentration-dependent behavior of rGO-AuNP electrodes modified with anti-IgG antibodies until interface saturation (Fig. 2B). It suggests the potential of rGO-AuNP electrodes as transducer platforms for detecting glycoproteins, including our target, the CA-19-9 glycoprotein.

Expanding the proof-of-concept to detect cancer biomarker glycoproteins, it's important to note that CA-19-9 standards come from pretreated CA-19-9 antigens from human fluids, as outlined by the manufacturer and detailed in the SI methodology. Consequently, the $C_{\bar{\mu}}$ biosensor response of the blank sample (0 U mL^{-1}) slightly decreased to ~229 ± 7 μF cm^{-2} attributed to the sample matrix effect (Cecchetto et al., 2017, 2020; Echeverri et al., 2023). Furthermore, the antibody-glycoprotein biorecognition event at the nanostructured interface led to perturbation in electronic DOS, and $C_{\bar{\mu}}$ decreased to ~214 ± 6 μF cm^{-2} (Lucas Garrote et al., 2022). Real capacitance values for rGO-AuNP electrode modified with anti-CA-19-9 antibody, after blocking non-specific adsorption sites with BSA and after interaction with blank and target samples, respectively, are shown in Fig. 3B. Notably, the nanobiosensor exhibited statistically significant differences upon interaction with CA-19-9 glycoprotein compared to the blank sample ($p < 0.05$).

In addition to the capacitive Nyquist plots shown in Figs. 2A and 3A, acquired data was represented by capacitive Bode plots, showing the frequency-resolved influence of rGO-AuNPs charging on real and imaginary capacitive elements (Lehr et al., 2014). Bode plots of real capacitance depict the quantum capacitance as a charging plateau (Figs. 2C and 3C). Instead, the imaginary component is a transient peak with a maximum at a frequency that correlates directly to the rate of electron flow across the rGO π-conjugated orbitals (Figs. 2D and 3D) (Gutierrez et al., 2017; Lehr et al., 2014). Real capacitance is highly dependent on the electronic DOS, and biorecognition molecular events at the nanostructured interface perturb the DOS, hence C' decreased, indicating a successful antibody-glycoprotein molecular binding (Bueno et al., 2015; Lehr et al., 2014). Furthermore, C'' decreased after each step of the biosensing interface assembly, like the trend obtained for C'. This result agrees with reports in the literature for capacitive biosensors (Fernandes et al., 2013; Fernandes and Bueno, 2017; Lehr et al., 2014; Marques et al., 2015).

Moreover, we characterized the biosensing interface assembly for detecting CA-19-9 glycoprotein by CV and EIS using the ferro/ferricyanide couple as a redox probe in a buffered solution (Fig. S2). The results

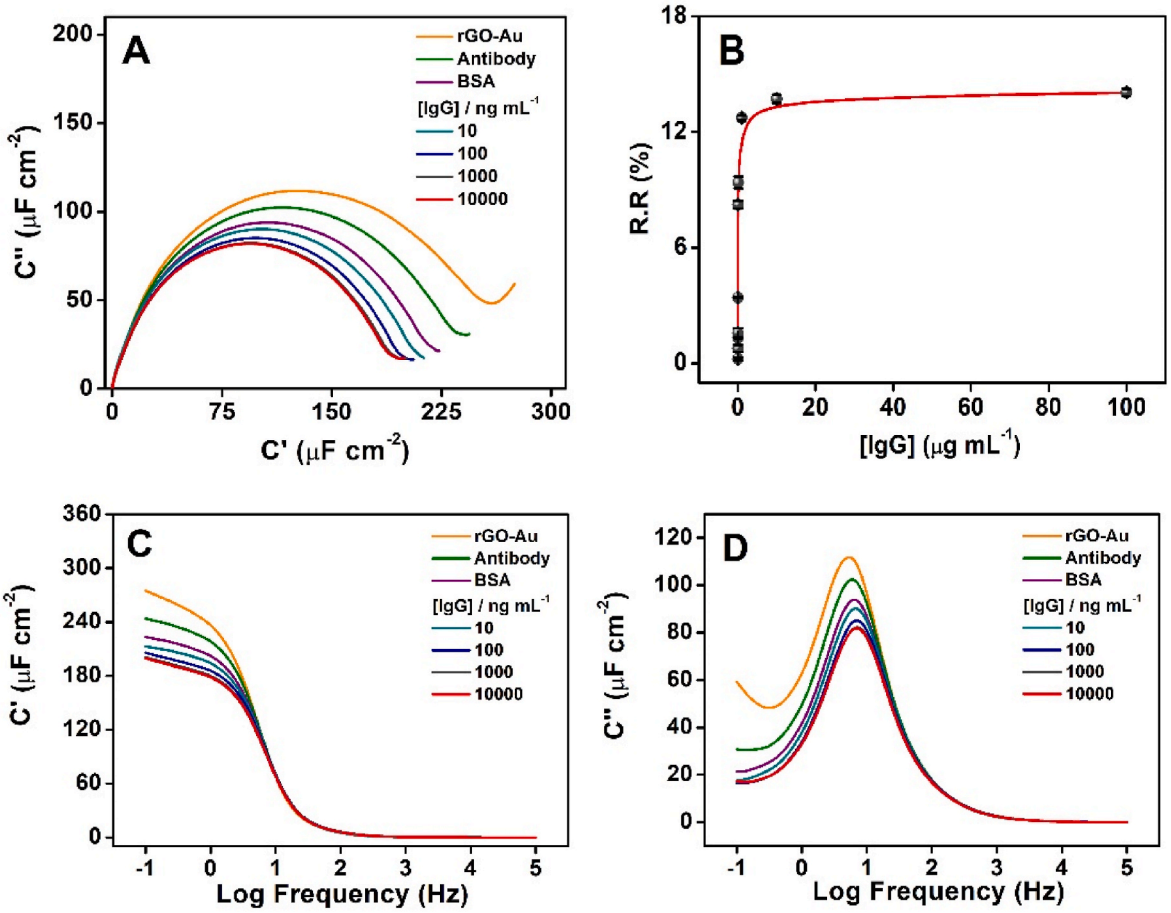

Fig. 2. Electrochemical characterization of the IgG biosensing interface assembly by ECS. **A**) Capacitive Nyquist plots in 50 mM PBS/0.1 M KCl pH 6.0, 10 mV amplitude sinusoidal perturbation, frequency range from 100 kHz to 0.1 Hz. The yellow line is the bare rGO-AuNPs electrode, green is the rGO-AuNPs with the anti-IgG antibody adsorbed onto the surface, purple is the rGO-AuNPs/antibody with BSA, and dark cyan, blue, dark gray, and red is the human IgG recruited onto the biosensing interface at concentrations of 10, 100, 1000 and 10000 ng mL^{-1}, respectively. **B**) Biosensor relative response to different IgG concentrations calculated as $RR\ (\%) = [(1/C_{\bar{\mu}\,(IgG)} - 1/C_{\bar{\mu}\,(BSA)})/1/C_{\bar{\mu}\,(BSA)}]\ x\ 100$. **C**) Bode plots of the real capacitance (C′). **D**) Bode plots of the imaginary capacitance (C″).

obtained by CV showed how the interfacial electrical properties changed as the biosensor was assembled (Fig. S2A). However, these interfacial electrical changes were more evident when characterized by EIS; with this technique, significant changes in R_{ct} were observed after each biosensing interface assembly step, as shown in Fig. S2B. The interfacial electrical changes indicated the successful biomolecule immobilization onto the rGO-AuNPs surface, thus hindering the electron transfer from the soluble redox probe to the rGO-AuNPs surface, increasing the R_{ct} (see Table S3) (Echeverri and Orozco, 2022b).

In addition, we monitored the nanobiosensor assembly by XPS after the electrode fabrication process, antibody immobilization, blocking with BSA, and CA-19-9 recruiting to confirm the successful biofunctionalization process. The high-resolution C1s spectrum of antibodies attached to the rGO-AuNPs surface showed characteristic peaks at 286.4 and 288.6 eV of peptide chains of the immunoglobulin G structure (Gruian et al., 2012; Lebugle et al., 1995), absent in the spectrum of the nanostructured rGO-AuNPs surface (Fig. S3 A-B). These peaks confirmed the successful antibody adsorption onto the rGO-AuNPs surface. Table S4 shows the peak area corresponding to each component of the biosensing interface. The peak areas corresponding to peptide chains increased upon adding BSA and target glycoprotein recruitment, confirming the successful biorecognition event at the nanostructured interface (Fig. S3 C-D). Concerning the quantum capacitance of the rGO-AuNP nanostructured interface, we observed a notable decrease in C-C, C=C, and C-O corresponding peak areas after antibody adsorption, BSA blocking, and target glycoprotein recognition. These peaks are associated with sp^2 and sp^3 carbon hybridization. The decrease in peak area agreed with the results obtained by ECS. We observed a fall in $C_{\bar{\mu}}$ after each modification step with the biomolecules related to the perturbation of localized and non-localized electronic states in the conjugated π-orbital system of the rGO-AuNPs molecular structure (Gutierrez et al., 2017), the electrochemical characterization and XPS analysis confirmed the successful assembly of the nanobiosensing interface. In summary, all results demonstrated the successful assembly of the biosensing interfaces for IgG antibodies and CA-19-9 glycoprotein detection.

3.3. Biosensor analytical performance

After confirming the nanobiosensor's capability for glycoprotein detection, we assessed the analytical performance by analyzing different standard solutions containing known concentrations of CA-19-9 ranging from 0 to 300 U mL^{-1} (Fig. 4A). It is important to highlight that we used standard solutions with known CA-19-9 glycoprotein concentrations from an ELISA kit. The manufacturer prepared the standards from a partially purified CA-19-9 antigen using human fluids as the source. Therefore, the standard solution corresponding to 0 U mL^{-1} provided by the manufacturer enabled us to consider the background signal related to the sample matrix (blank sample). As previously discussed, localized and non-localized electronic states in the conjugated π-orbital system of the rGO molecular structure and capacitive charging are altered by glycoprotein-antibody interaction (Lucas Garrote et al., 2022). The

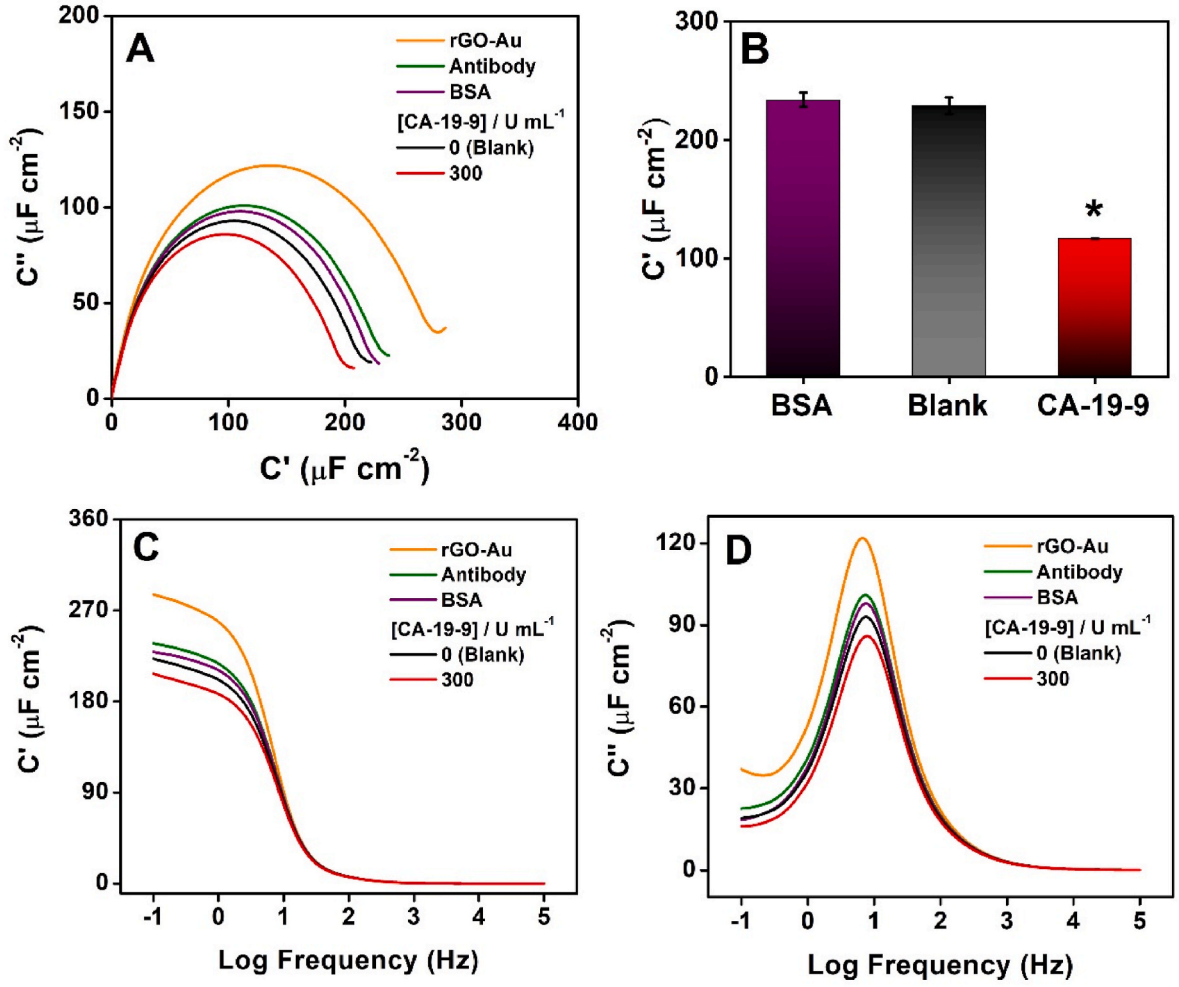

Fig. 3. Electrochemical characterization of the CA-19-9 biosensing interface assembly by ECS. **A**) Capacitive Nyquist plots in 50 mM PBS/0.1 M KCl pH 6.0, 10 mV amplitude sinusoidal perturbation, frequency range from 100 kHz to 0.1 Hz. The yellow line is the bare rGO-AuNPs electrode, green is the rGO-AuNPs with the anti-CA-19-9 antibody adsorbed onto the surface, purple is the rGO-AuNPs/Antibody with BSA, black is the blank sample and red is the CA-19-9 glycoprotein recruited onto the biosensing interface at a concentration of 300 U mL^{-1}, respectively. **B**) Real capacitance values for the rGO-AuNPs electrode were modified with an anti-CA-19-9 antibody, and non-specific adsorption sites were blocked with BSA after interacting with the blank and molecular target samples, respectively. * Significantly different concerning blank sample ($p < 0.05$). **C**) Bode plots of the real capacitance (C′). **D**) Bode plots of the imaginary capacitance (C″).

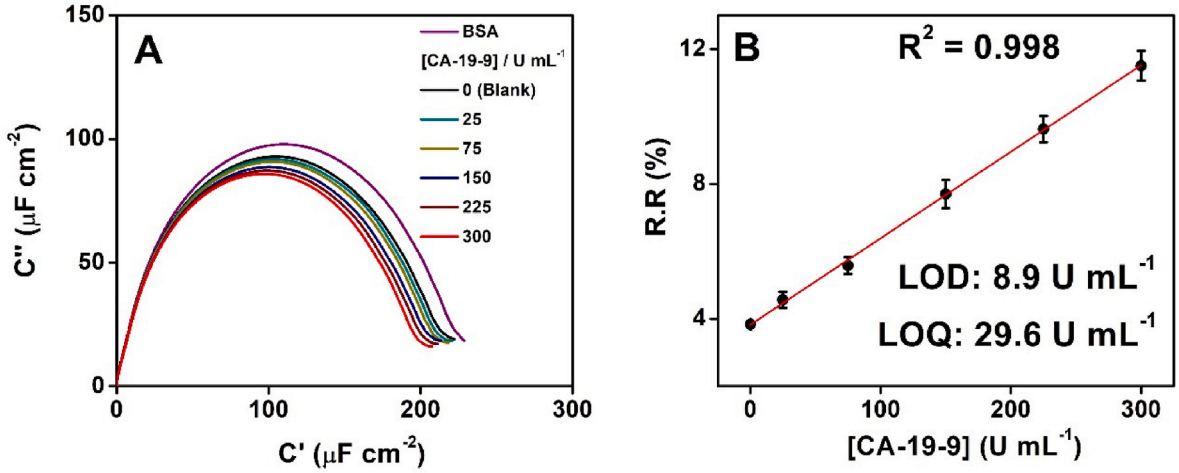

Fig. 4. **A**) Capacitive Nyquist plots for different CA-19-9 glycoprotein concentrations, from 0 to 300 U mL^{-1} **B**) Resultant calibration curve using the relative variation of electrochemical capacitance as a transducing signal.

capacitance response decreased with increasing CA-19-9 glycoprotein concentration, displaying a linear correlation suitable for analytical purposes (Marques et al., 2015). Consequently, a calibration curve was generated by calculating the relative response (RR %) for each glycoprotein concentration, showing a linear correlation with the CA-19-9 glycoprotein concentration from 0 to 300 U mL^{-1} described by the equation RR (%) = 0.026 * [CA-19-9] + 3.82 with a correlation coefficient R^2 = 0.998 (Fig. 4B).

The calculated limit of detection (LOD) was established at 8.9 U mL^{-1}, while the limit of quantification (LOQ) was set at 29.6 U mL^{-1}, based on the 3-sigma and 10-sigma criteria, respectively. These parameters are significant in clinical diagnosis, where a CA-19-9 glycoprotein level below 37 U mL^{-1} is deemed normal for healthy individuals, while an equal or elevated level indicates an increased value associated with cancer (Kim et al., 2004; Lakemeyer et al., 2021; Thomsen et al., 2018). Our nanobiosensor demonstrated accuracy and rapid response in detecting these levels, underscoring its utility. These analytical attributes suggest that the capacitive nanobiosensor, leveraging rGO-AuNPs, holds potential for clinical application in detecting CA-19-9 glycoprotein within a label-free and reagentless operational framework.

3.4. Biosensor specificity, stability, repeatability, and reproducibility

To assess nanobiosensor specificity, we gauged its capacitive response towards biomolecules that could potentially interfere with CA-19-9 glycoprotein detection. We conducted this evaluation to ascertain the potential cross-reactivity of the anti-CA-19-9 antibody to several biomolecules, including CEA, p53 antigen, anti-p53 and IgG antibodies, and β-1,4-galactosyltransferase-V (β-1,4-GalT-V) glycoprotein. The CEA and p53 antigens, anti-p53 antibody, and β-1,4-GalT-V are proteins overexpressed during colorectal cancer tumorigenesis and released from tumor cells to body fluids (Echeverri et al., 2023; Quinchia et al., 2020). As the most abundant antibody in human blood (Schroeder et al., 2010) IgG, alongside CEA, p53, anti-p53, and β-1,4-GalT-V, bears the potential to interact with the anti-CA-19-9 antibody, potentially yielding false-negative outcomes. Fig. 5 showcases RR (%) acquired from ECS measurements. Significantly higher RR (%) was observed for CA-19-9 glycoprotein (7.70 ± 0.42) compared to CEA (3.63 ± 0.45), β-1, 4-GalT-V (3.82 ± 0.22), p53 (4.20 ± 0.02), anti-p53 antibody (4.31 ± 0.46), and IgG (3.88 ± 0.52). The statistical differences in signals (RR %) for CA-19-9 glycoprotein in comparison to blank and other tested proteins, whether individual or mixed, were evident through 1-way ANOVA analysis with a 95% level of statistical significance ($p < 0.05$). Notably, the device assembly exhibited high inter-electrodes reproducibility (Fig. S4A), as evidenced by nanobiosensors assembled up to the BSA blocking step on five independent electrodes (RSD of $1/C_{\bar{\mu}\ BSA}$ = 2.67 %). We also assessed the interface stability of the nanobiosensor by monitoring the ECS response after we exposed it to the blank sample. After three consecutive measurements, the RR (%) was 3.77 ± 0.62 % for the blank (Fig. S4B). The corresponding RSD for the $1/C_{\bar{\mu}\ Blank}$ value was 0.60 %, thus confirming the high stability of the nanobiosensing interface. We evaluated the intra-electrode repeatability and inter-electrode reproducibility of our nanobiosensor to the target by measuring the ECS response of 300 U mL^{-1} of CA-19-9 glycoprotein. The repeatability and reproducibility, calculated as relative standard deviation (RSD), were 0.3 % (n = 3) and 5.8 % (n = 5), respectively. Although we did not perform long-term stability assays of the devices, they are usually limited by the biorecognition elements immobilized on the transducers under storage conditions (Cruz-Pacheco et al., 2024). Instead, to proof-the-concept we used freshly prepared biosensors because fresh preparation ensures the optimal integrity and functionality of the sensitive bioreceptor, mitigating potential compromises that might arise from prolonged storage.

The results demonstrated the specificity and selectivity of the nanobiosensor, likely showing how it responds to CA-19-9 in the presence of interfering proteins. The nanobiosensor response has been

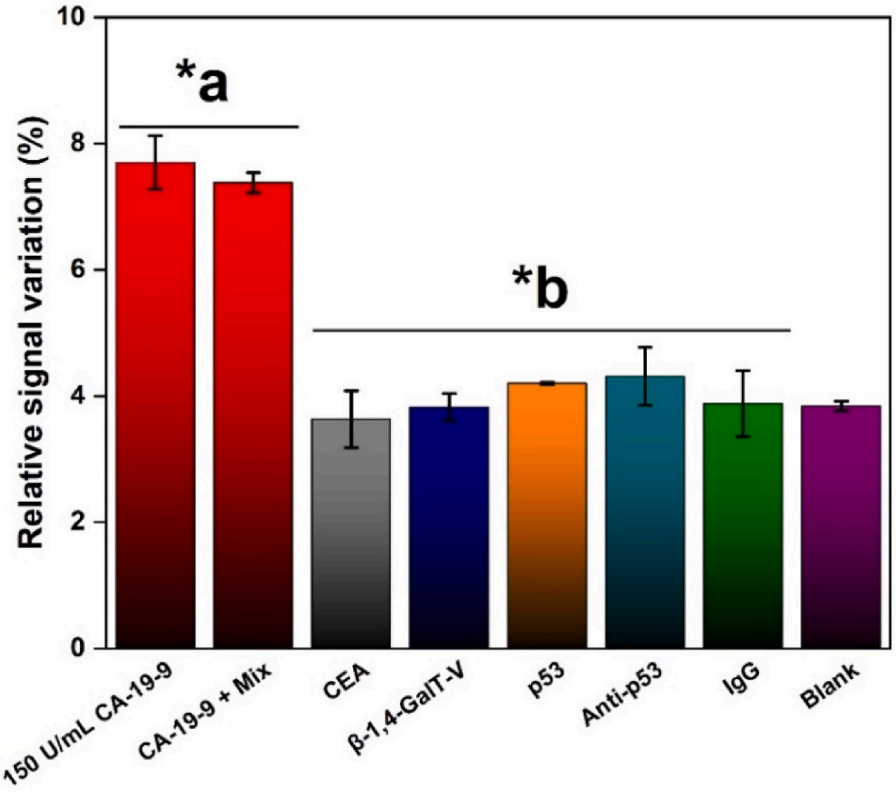

Fig. 5. Relative signal variation for 150 U mL^{-1} of CA-19-9 in the presence of 10 ng mL^{-1} of CEA and p53 antigens, anti-p53 and IgG antibodies, and β-1,4-GalT-V glycoprotein. Statistically significant difference ***a** concerning the blank sample ($p < 0.05$) and ***b** to the 150 U mL^{-1} CA-19-9 sample ($p < 0.05$).

evaluated at 150 U mL^{-1} of CA-19-9 with various interferents, achieving a signal-to-noise (S/N) ratio above 2 and showing a reliable response. However, this concentration marks the midpoint of the calibration curve. Remarkably, the sensor achieved a maximal S/N ratio at the highest detected concentration of 300 U mL^{-1} (S/N = 3), implying that the sensor can reliably detect higher concentrations with better accuracy, helpful in a potential practical application. Yet, different strategies could be implemented to improve the S/N ratio, for example, by a recently reported capacitance amplification mechanism (Garrote et al., 2024) based on modifying the rGO-AuNPs electrode by covalently attaching ferrocene (Fc) while additionally introducing Fc in solution. Furthermore, novel signal amplification strategies based on CRISPR-Cas technology could be explored (N. Liu et al., 2022).

3.5. Recovery assay of CA-19-9 in serum samples

To evaluate the accuracy of the capacitive biosensor in quantifying the CA-19-9 biomarker in serum samples, we performed a recovery assay using the spike methodology (Garrote et al., 2024). The response of the biosensing interface to three concentrations of CA-19-9 was evaluated, as described in detail in supporting information. The CA-19-9 concentrations were measured by substituting the RR% of each sample in the analytical curve of Fig. 4B, with an analytical recovery (%) compiled in Table 1. The results indicate that the AR% for all three samples shows a high recovery of the target glycoprotein, close to 100%. However, the case with a concentration of 30 U mL^{-1} demonstrates slight inaccuracy, attributed to the proximity of this concentration to the LOQ of the assay (Garrote et al., 2024). Regardless of the inaccuracy in estimating lower concentrations, it was possible to demonstrate quantum capacitive immunosensing of CA-19-9 biomarker at laser-engraved graphene electrodes. Even though other reported biosensors for CA-19-9 detection with other electrochemical methods compiled in Table S5 achieve lower LODs than our nanobiosensor, it can detect the biomarker in undiluted human serum at concentrations of clinical relevance and a more comprehensive working range concerning some previous works.

4. Conclusions

In this study, we have pioneered the development of a novel capacitive biosensor tailored for glycoproteins, leveraging laser-engraved reduced graphene oxide electrodes decorated with AuNPs. The fabrication involved precise laser-scribing of GO-Au^{3+} films, yielding rGO-AuNP electrodes seamlessly transferred onto a PET sheet using a press-stamping technique and subsequently functionalized with specific bioreceptors. Initially, we validated the biosensor's performance by successfully detecting human IgG antibodies, thus confirming its biomolecular recognition capabilities. Subsequently, our focus shifted to detecting CA-19-9 glycoprotein, a critical clinical biomarker, thereby showcasing the practical applicability of our capacitive biosensing approach.

Our nanobiosensor demonstrated robust monitoring of CA-19-9 glycoprotein concentrations relevant to clinical contexts. The biosensor's selectivity was verified by evaluating potential cross-reactivity with various biomolecules. Our comprehensive testing established its ability to discern CA-19-9 glycoprotein with minimal interference from other analytes. These findings underscore the precision, specificity, and reliability of rGO-AuNP biosensors in accurately quantifying glycoproteins, highlighting their reproducibility and stability. Their adaptability to detect a wide range of biomolecules positions them as versatile tools for point-of-care applications, ultimately promising to enhance healthcare accessibility and patient-centered outcomes significantly.

CRediT authorship contribution statement

Danilo Echeverri: Writing – original draft, Methodology, Investigation, Data curation. **Enric Calucho:** Writing – original draft, Methodology. **Jose Marrugo-Ramírez:** Software, Data curation. **Ruslán Álvarez-Diduk:** Writing – review & editing, Supervision, Conceptualization. **Jahir Orozco:** Writing – review & editing, Supervision. **Arben Merkoçi:** Writing – review & editing, Supervision.

Table 1
CA-19-9 recovery assays performed by capacitive immunodetection. The experiments were performed in duplicate.

$[CA\text{-}19\text{-}9]_{Spiked}$/U mL^{-1}	$[CA\text{-}19\text{-}9]_{Measured}$/U mL^{-1}	Accuracy rate (%)
30	30 ± 9	99 ± 31
150	149 ± 1	99 ± 1
300	290 ± 2	97 ± 1

Declaration of competing interest

The authors declare that they have no known competing financial interests or personal relationships that could have appeared to influence the work reported in this paper.

Data availability

No data was used for the research described in the article.

Acknowledgments

The ICN2 is funded by the CERCA programme/Generalitat de Catalunya. The ICN2 is supported by the Severo Ochoa Centres of Excellence program, Grant CEX2021-001214-S, funded by MCIN/AEI/10.13039.501100011033. Minciencias partially funded the work through the project Cod. 111593092980. This project has received funding from the European Union's Horizon 2020 research and innovation programme under grant agreement No 881603. Views and opinions expressed are, however, those of the author(s) only and do not necessarily reflect those of the European Union. The European Union can not be held responsible for them. JO thanks support from The University of Antioquia and the Max Planck Society through the cooperation agreement 566–1, 2014. We thank The Ruta N complex for hosting the Max Planck Tandem Groups. E. Calucho acknowledges Ministerio de Ciencia e Innovación of Spain and Fondo Social Europeo for the Fellowship PRE2018-084856 awarded under the call "Ayudas para contratos predoctorales para la formación de doctores, Subprograma Estatal de Formación del Programa Estatal de Promoción del Talento y su Empleabilidad en I+D+i", under the framework of "Plan Estatal de Investigación Científica y Técnica y de Innovación 2017–2020". E. Calucho also acknowledges Universitat Autònoma de Barcelona (UAB) for the support and the possibility of performing this work within the framework of the Biotechnology PhD Programme.

Appendix A. Supplementary data

Supplementary data to this article can be found online at https://doi.org/10.1016/j.bios.2024.116142.

References

Allison, A., Andreas, H.A., 2019. Minimizing the Nyquist-plot semi-circle of pseudocapacitive manganese oxides through modification of the oxide-substrate interface resistance. J. Power Sources 426, 93–96. https://doi.org/10.1016/j.jpowsour.2019.04.029.

Ambaye, A.D., Kefeni, K.K., Mishra, S.B., Nxumalo, E.N., Ntsendwana, B., 2021. Recent developments in nanotechnology-based printing electrode systems for electrochemical sensors. Talanta 225, 121951. https://doi.org/10.1016/j.talanta.2020.121951.

Amouzadeh Tabrizi, M., Acedo, P., 2022. An electrochemical immunosensor for the determination of procalcitonin using the gold-graphene interdigitated electrode. Biosensors 12, 771. https://doi.org/10.3390/bios12100771.

Antuña-Jiménez, D., González-García, M.B., Hernández-Santos, D., Fanjul-Bolado, P., 2020. Screen-printed electrodes modified with metal nanoparticles for small

molecule sensing, 2020 Biosensors 10. https://doi.org/10.3390/bios10020009. Page 9 10, 9.
Arduini, F., Micheli, L., Moscone, D., Palleschi, G., Piermarini, S., Ricci, F., Volpe, G., 2016. Electrochemical biosensors based on nanomodified screen-printed electrodes: recent applications in clinical analysis. TrAC, Trends Anal. Chem. 79, 114–126. https://doi.org/10.1016/j.trac.2016.01.032.
Barman, S.C., Zahed, MdA., Sharifuzzaman, Md, Ko, S.G., Yoon, H., Nah, J.S., Xuan, X., Park, J.Y., 2020. Immunosensing platforms: a polyallylamine anchored amine-rich laser-ablated graphene platform for facile and highly selective electrochemical IgG biomarker detection (adv. Funct. Mater. 14/2020). Adv. Funct. Mater. 30, 2070093 https://doi.org/10.1002/adfm.202070093.
Barsan, M.M., Brett, C.M.A., 2016. Recent advances in layer-by-layer strategies for biosensors incorporating metal nanoparticles. TrAC, Trends Anal. Chem. 79, 286–296. https://doi.org/10.1016/j.trac.2015.11.019.
Bueno, P.R., 2019. Nanoscale origins of super-capacitance phenomena. J. Power Sources 414, 420–434. https://doi.org/10.1016/j.jpowsour.2019.01.010.
Bueno, P.R., Davis, J.J., 2020. Charge transport and energy storage at the molecular scale: from nanoelectronics to electrochemical sensing. Chem. Soc. Rev. 49, 7505–7515. https://doi.org/10.1039/C9CS00213H.
Bueno, P.R., Davis, J.J., 2014. Measuring quantum capacitance in energetically addressable molecular layers. Anal. Chem. 86, 1337–1341. https://doi.org/10.1021/ac403135b.
Bueno, P.R., Feliciano, G.T., Davis, J.J., 2015. Capacitance spectroscopy and density functional theory. Phys. Chem. Chem. Phys. 17, 9375–9382. https://doi.org/10.1039/C4CP06015F.
Campuzano, S., Pedrero, M., Yáñez-Sedeño, P., Pingarrón, J.M., 2021. New challenges in point of care electrochemical detection of clinical biomarkers. Sensor. Actuator. B Chem. 345 https://doi.org/10.1016/j.snb.2021.130349.
Cecchetto, J., Fernandes, F.C.B., Lopes, R., Bueno, P.R., 2017. The capacitive sensing of NS1 Flavivirus biomarker. Biosens. Bioelectron. 87, 949–956. https://doi.org/10.1016/j.bios.2016.08.097.
Cecchetto, J., Santos, A., Mondini, A., Cilli, E.M., Bueno, P.R., 2020. Serological point-of-care and label-free capacitive diagnosis of dengue virus infection. Biosens. Bioelectron. 151, 111972 https://doi.org/10.1016/j.bios.2019.111972.
Chandra Barman, S., Sharifuzzaman, M., Zahed, M.A., Park, C., Yoon, S.H., Zhang, S., Kim, H., Yoon, H., Park, J.Y., 2021. A highly selective and stable cationic polyelectrolyte encapsulated black phosphorene based impedimetric immunosensor for Interleukin-6 biomarker detection. Biosens. Bioelectron. 186, 113287 https://doi.org/10.1016/j.bios.2021.113287.
Cruz-Pacheco, A.F., Echeverri, D., Orozco, J., 2024. Role of electrochemical nanobiosensors in colorectal cancer precision medicine. TrAC, Trends Anal. Chem. 170, 117467 https://doi.org/10.1016/j.trac.2023.117467.
Cruz-Pacheco, A.F., Quinchia, J., Orozco, J., 2023. Nanostructured poly(thiophene acetic acid)/Au/poly(methylene blue) interface for electrochemical immunosensing of p53 protein. Microchim. Acta 190, 1–12. https://doi.org/10.1007/s00604-023-05683-5.
Echeverri, D., Cruz-Pacheco, A.F., Orozco, J., 2023. Capacitive nanobiosensing of β-1,4-galactosyltransferase-V colorectal cancer biomarker. Sensor. Actuator. B Chem. 374, 132784 https://doi.org/10.1016/j.snb.2022.132784.
Echeverri, D., Orozco, J., 2022a. Glycan-based electrochemical biosensors: promising tools for the detection of infectious diseases and cancer biomarkers, 2022 Molecules 27, 8533. https://doi.org/10.3390/molecules27238533. Page 8533 27.
Echeverri, D., Orozco, J., 2022b. β-1,4-Galactosyltransferase-V colorectal cancer biomarker immunosensor with label-free electrochemical detection. Talanta 243, 123337. https://doi.org/10.1016/j.talanta.2022.123337.
Elgrishi, N., Rountree, K.J., McCarthy, B.D., Rountree, E.S., Eisenhart, T.T., Dempsey, J. L., 2018. A practical beginner's guide to cyclic voltammetry. J. Chem. Educ. 95, 197–206. https://doi.org/10.1021/acs.jchemed.7b00361.
Fernandes, F.C.B., Bueno, P.R., 2017. Optimized electrochemical biosensor for human prostatic acid phosphatase. Sensor. Actuator. B Chem. 253, 1106–1112. https://doi.org/10.1016/j.snb.2017.06.035.
Fernandes, F.C.B., Góes, M.S., Davis, J.J., Bueno, P.R., 2013. Label free redox capacitive biosensing. Biosens. Bioelectron. 50, 437–440. https://doi.org/10.1016/j.bios.2013.06.043.
Fernández-Sánchez, C., Pellicer, E., Orozco, J., Jiménez-Jorquera, C., Lechuga, L.M., Mendoza, E., 2009. Plasma-activated multi-walled carbon nanotube–polystyrene composite substrates for biosensing. Nanotechnology 20, 335501. https://doi.org/10.1088/0957-4484/20/33/335501.
Gao, S., Guisán, J.M., Rocha-Martin, J., 2022. Oriented immobilization of antibodies onto sensing platforms - a critical review. Anal. Chim. Acta. https://doi.org/10.1016/j.aca.2021.338907.
Garrote, B.L., Sánchez, Y.P., Lopes, L.C., Santos, A., Bueno, P.R., 2024. Electron transmittance by means of quantum capacitive states as a signal amplification mechanism for biosensing applications. Sensor. Actuator. B Chem. 399 https://doi.org/10.1016/j.snb.2023.134786.
Garrote, B.L., Santos, A., Bueno, P.R., 2020. Label-free capacitive assaying of biomarkers for molecular diagnostics. Nat. Protoc. 15 (12 15), 3879–3893. https://doi.org/10.1038/s41596-020-0390-9, 2020.
Ghildiyal, P., Yang, Y., Kline, D.J., Holdren, S., Zachariah, M.R., 2019. Ultrafast, scalable laser photothermal synthesis and writing of uniformly dispersed metal nanoclusters in polymer films. Nanoscale 11, 13354–13365. https://doi.org/10.1039/C9NR02839K.
Giacomelli, C., Álvarez-Diduk, R., Testolin, A., Merkoçi, A., 2020. Selective stamping of laser scribed rGO nanofilms: from sensing to multiple applications. 2D Mater. 7, 024006 https://doi.org/10.1088/2053-1583/ab68a7.
Gruian, C., Vanea, E., Simon, S., Simon, V., 2012. FTIR and XPS studies of protein adsorption onto functionalized bioactive glass. Biochim. Biophys. Acta, Proteins Proteomics 1824, 873–881. https://doi.org/10.1016/j.bbapap.2012.04.008.
Guo, L., Li, X., Chen, G., 2010. Techniques of electrode fabrication. Electrochemistry for the Environment 55–98. https://doi.org/10.1007/978-0-387-68318-8_3.
Gupta, Y., Pandey, C.M., Ghrera, A.S., 2022. Reduced graphene oxide-gold nanoparticle nanohybrid modified cost-effective paper-based biosensor for procalcitonin detection. ChemistrySelect 7, e202202642. https://doi.org/10.1002/SLCT.202202642.
Gutierrez, F.A., Bedatty Fernandes, F.C., Rivas, G.A., Bueno, P.R., 2017. Mesoscopic behaviour of multi-layered graphene: the meaning of supercapacitance revisited. Phys. Chem. Chem. Phys. 19, 6792–6806. https://doi.org/10.1039/C6CP07775G.
Hoogvliet, J.C., Dijksma, M., Kamp, B., van Bennekom, W.P., 2000. Electrochemical pretreatment of polycrystalline gold electrodes to produce a reproducible surface roughness for self-assembly: a study in phosphate buffer pH 7.4. Anal. Chem. 72, 2016–2021. https://doi.org/10.1021/ac991215y.
Hou, C., Luo, Q., He, Y., Zhang, H., 2021. Potentiostatic electrodeposition of gold nanoparticles: variation of electrocatalytic activity toward four targets. J. Appl. Electrochem. 51, 1721–1730. https://doi.org/10.1007/s10800-021-01604-7.
Huang, Y., Hara, A., Terashima, C., Fujishima, A., Takai, M., 2019. Protein adsorption behavior on reduced graphene oxide and boron-doped diamond investigated by electrochemical impedance spectroscopy. Carbon N Y 152, 354–362. https://doi.org/10.1016/j.carbon.2019.06.023.
Hui, J., Zhou, X., Bhargava, R., Chinderle, A., Zhang, J., Rodríguez-López, J., 2016. Kinetic modulation of outer-sphere electron transfer reactions on graphene electrode with a sub-surface metal substrate. Electrochim. Acta 211, 1016–1023. https://doi.org/10.1016/j.electacta.2016.06.134.
Iamprasertkun, P., Dryfe, R.A.W., 2019. The capacitance of graphene: from model systems to large-scale devices. Nanocarbon Electrochemistry 33–84. https://doi.org/10.1002/9781119468288.ch2.
Khalil, I., Rahmati, S., Muhd Julkapli, N., Yehye, W.A., 2018. Graphene metal nanocomposites — recent progress in electrochemical biosensing applications. J. Ind. Eng. Chem. 59, 425–439. https://doi.org/10.1016/j.jiec.2017.11.001.
Kim, J.E., Lee, K.T., Lee, J.K., Paik, S.W., Rhee, J.C., Choi, K.W., 2004. Clinical usefulness of carbohydrate antigen 19-9 as a screening test for pancreatic cancer in an asymptomatic population. J. Gastroenterol. Hepatol. 19, 182–186. https://doi.org/10.1111/j.1440-1746.2004.03219.x.
Kim, Y.K., Na, H.K., Lee, Y.W., Jang, H., Han, S.W., Min, D.H., 2010. The direct growth of gold rods on graphene thin films. Chem. Commun. 46, 3185–3187. https://doi.org/10.1039/C002002H.
Lahcen, A.A., Rauf, S., Beduk, T., Durmus, C., Aljedaibi, A., Timur, S., Alshareef, H.N., Amine, A., Wolfbeis, O.S., Salama, K.N., 2020. Electrochemical sensors and biosensors using laser-derived graphene: a comprehensive review. Biosens. Bioelectron. 168, 112565 https://doi.org/10.1016/j.bios.2020.112565.
Lakemeyer, L., Sander, S., Wittau, M., Henne-Bruns, D., Kornmann, M., Lemke, J., Esposito, F., 2021. Diagnostic and prognostic value of CEA and CA19-9 in colorectal cancer, 2021 Diseases 9, 21. https://doi.org/10.3390/diseases9010021. Page 21 9.
Lazanas, A.C., Prodromidis, M.I., 2023. Electrochemical Impedance Spectroscopy—A Tutorial. ACS Measurement Science Au. https://doi.org/10.1021/acsmeasuresciau.2c00070.
Lebugle, A., Subirade, M., Gueguen, J., 1995. Structural characteristics of a globular protein investigated by X-ray photoelectron spectroscopy: comparison between a legumin film and a powdered legumin. Biochim. Biophys. Acta. https://doi.org/10.1016/0167-4838(95)00009-J.
Lehr, J., Fernandes, F.C.B., Bueno, P.R., Davis, J.J., 2014. Label-free capacitive diagnostics: exploiting local redox probe state occupancy. Anal. Chem. 86, 2559–2564. https://doi.org/10.1021/ac403727h.
Li, G., 2020. Direct laser writing of graphene electrodes. J. Appl. Phys. 127, 010901 https://doi.org/10.1063/1.5120056.
Liu, J., Peng, Q., 2017. Protein-gold nanoparticle interactions and their possible impact on biomedical applications. Acta Biomater. 55, 13–27. https://doi.org/10.1016/j.actbio.2017.03.055.
Liu, J., Zhu, B., Dong, H., Zhang, Y., Xu, M., Travas-Sejdic, J., Chang, Z., 2022. A novel electrochemical insulin aptasensor: from glassy carbon electrodes to disposable, single-use laser-scribed graphene electrodes. Bioelectrochemistry 143. https://doi.org/10.1016/j.bioelechem.2021.107995.
Liu, N., Liu, R., Zhang, J., 2022. CRISPR-Cas12a-mediated label-free electrochemical aptamer-based sensor for SARS-CoV-2 antigen detection. Bioelectrochemistry 146. https://doi.org/10.1016/j.bioelechem.2022.108105.
Liu, X., Lin, L.Y., Tseng, F.Y., Tan, Y.C., Li, J., Feng, L., Song, L., Lai, C.F., Li, X., He, J.H., Sakthivel, R., Chung, R.J., 2021. Label-free electrochemical immunosensor based on gold nanoparticle/polyethyleneimine/reduced graphene oxide nanocomposites for the ultrasensitive detection of cancer biomarker matrix metalloproteinase-1. Analyst 146, 4066–4079. https://doi.org/10.1039/D1AN00537E.
Lopes, L.C., Santos, A., Bueno, P.R., 2022. An outlook on electrochemical approaches for molecular diagnostics assays and discussions on the limitations of miniaturized technologies for point-of-care devices. Sensors and Actuators Reports 4, 100087. https://doi.org/10.1016/j.snr.2022.100087.
Lopes, L.C., Santos, A., Bueno, P.R., 2021. Measuring quantum conductance and capacitance of graphene using impedance-derived capacitance spectroscopy. Carbon N Y 184, 821–827. https://doi.org/10.1016/j.carbon.2021.08.055.
Lu, L., Seenivasan, R., Wang, Y.C., Yu, J.H., Gunasekaran, S., 2016. An electrochemical immunosensor for rapid and sensitive detection of mycotoxins fumonisin B1 and deoxynivalenol. Electrochim. Acta 213, 89–97. https://doi.org/10.1016/j.electacta.2016.07.096.

Lucas Garrote, B., Lopes, L.C., Pinzón, E.F., Mendonça-Natividade, F.C., Martins, R.B., Santos, A., Arruda, E., Bueno, P.R., 2022. Reagentless quantum-rate-based electrochemical signal of graphene for detecting SARS-CoV-2 infection using nasal swab specimens. ACS Sens. 7, 2645–2653. https://doi.org/10.1021/acssensors.2c01016.

Luo, Y., Wu, S., Xiang, X., Shu, J., Fei, J., 2023. Fabricating process-electrochemical property correlation of laser-scribed graphene and smartphone-based electrochemical platform for portable and sensitive biosensing. Biosens. Bioelectron. 237, 115525 https://doi.org/10.1016/j.bios.2023.115525.

Marques, S.M., Santos, A., Gonçalves, L.M., Sousa, J.C., Bueno, P.R., 2015. Sensitive label-free electron chemical capacitive signal transduction for D-dimer electroanalysis. Electrochim. Acta 182, 946–952. https://doi.org/10.1016/j.electacta.2015.09.169.

Mendoza, E., Orozco, J., Jiménez-Jorquera, C., González-Guerrero, A.B., Calle, A., Lechuga, L.M., Fernández-Sánchez, C., 2008. Scalable fabrication of immunosensors based on carbon nanotube polymer composites. Nanotechnology 19, 075102. https://doi.org/10.1088/0957-4484/19/7/075102.

Moreira, G., Qian, H., Datta, S.P.A., Bliznyuk, N., Carpenter, J., Dean, D., McLamore, E., Vanegas, D., 2023. A capacitive laser-induced graphene based aptasensor for SARS-CoV-2 detection in human saliva. PLoS One 18. https://doi.org/10.1371/journal.pone.0290256.

Muzyka, K., Xu, G., 2022. Laser-induced Graphene in Facts, Numbers, and Notes in View of Electroanalytical Applications: A Review. Electroanalysis. https://doi.org/10.1002/elan.202100425.

Nah, J.S., Barman, S.C., Zahed, M.A., Sharifuzzaman, M., Yoon, H., Park, C., Yoon, S., Zhang, S., Park, J.Y., 2021. A wearable microfluidics-integrated impedimetric immunosensor based on Ti3C2Tx MXene incorporated laser-burned graphene for noninvasive sweat cortisol detection. Sensor. Actuator. B Chem. 329, 129206 https://doi.org/10.1016/j.snb.2020.129206.

Nemčeková, K., Labuda, J., 2021. Advanced materials-integrated electrochemical sensors as promising medical diagnostics tools: a review. Mater. Sci. Eng. C 120, 111751. https://doi.org/10.1016/j.msec.2020.111751.

Oliveira, R.M.B., Fernandes, F.C.B., Bueno, P.R., 2019. Pseudocapacitance phenomena and applications in biosensing devices. Electrochim. Acta 306, 175–184. https://doi.org/10.1016/j.electacta.2019.03.083.

Orozco, J., Suárez, G., Fernández-Sánchez, C., McNeil, C., Jiménez-Jorquera, C., 2007. Characterization of ultramicroelectrode arrays combining electrochemical techniques and optical microscopy imaging. Electrochim. Acta 53, 729–736. https://doi.org/10.1016/j.electacta.2007.07.049.

Peña-Bahamonde, J., Nguyen, H.N., Fanourakis, S.K., Rodrigues, D.F., 2018. Recent advances in graphene-based biosensor technology with applications in life sciences, 2018 J. Nanobiotechnol. 16 (1 16), 1–17. https://doi.org/10.1186/s12951-018-0400-z.

Prattis, I., Hui, E., Gubeljak, P., Kaminski Schierle, G.S., Lombardo, A., Occhipinti, L.G., 2021. Graphene for biosensing applications in point-of-care testing. Trends Biotechnol. 39, 1065–1077. https://doi.org/10.1016/j.tibtech.2021.01.005.

Quesada-González, D., Merkoçi, A., 2018. Nanomaterial-based devices for point-of-care diagnostic applications. Chem. Soc. Rev. 47, 4697–4709. https://doi.org/10.1039/C7CS00837F.

Quinchia, J., Echeverri, D., Cruz-Pacheco, A.F., Maldonado, M.E., Orozco, J.A., 2020. Electrochemical biosensors for determination of colorectal tumor biomarkers, 2020 Micromachines 11, 411. https://doi.org/10.3390/mi11040411. Page 411 11.

Rauf, S., Lahcen, A.A., Aljedaibi, A., Beduk, T., Ilton de Oliveira Filho, J., Salama, K.N., 2021a. Gold nanostructured laser-scribed graphene: a new electrochemical biosensing platform for potential point-of-care testing of disease biomarkers. Biosens. Bioelectron. 180 https://doi.org/10.1016/j.bios.2021.113116.

Rauf, S., Mani, V., Lahcen, A.A., Yuvaraja, S., Beduk, T., Salama, K.N., 2021b. Binary transition metal oxide modified laser-scribed graphene electrochemical aptasensor for the accurate and sensitive screening of acute myocardial infarction. Electrochim. Acta 386. https://doi.org/10.1016/j.electacta.2021.138489.

Ruiz, G., Ryan, N., Rutschke, K., Awotunde, O., Driskell, J.D., 2019. Antibodies irreversibly adsorb to gold nanoparticles and resist displacement by common blood proteins. Langmuir 35, 10601–10609. https://doi.org/10.1021/acs.langmuir.9b01900.

Schroeder, Cavacini, L., 2010. Structure and function of immunoglobulins. J. Allergy Clin. Immunol. 125 (2), S41–S52.

Scroccarello, A., Álvarez-Diduk, R., Pelle, F., Della, Silva, C. de C.C. e, Idili, A., Parolo, C., Compagnone, D., Merkoçi, A., 2023. One-step laser nanostructuration of reduced graphene oxide films embedding metal nanoparticles for sensing applications. ACS Sens. https://doi.org/10.1021/acssensors.2c01782.

Siriwardana, K., Wang, A., Vangala, K., Fitzkee, N., Zhang, D., 2013. Probing the effects of cysteine residues on protein adsorption onto gold nanoparticles using wild-type and mutated GB3 proteins. Langmuir 29, 10990–10996. https://doi.org/10.1021/la402239h.

Soares, R.R.A., Hjort, R.G., Pola, C.C., Parate, K., Reis, E.L., Soares, N.F.F., Mclamore, E. S., Claussen, J.C., Gomes, C.L., 2020. Laser-induced graphene electrochemical immunosensors for rapid and label-free monitoring of Salmonella enterica in chicken broth. ACS Sens. 5, 1900–1911. https://doi.org/10.1021/acssensors.9b02345.

Song, X., Wang, D., Kim, M., 2021. Development of an immuno-electrochemical glass carbon electrode sensor based on graphene oxide/gold nanocomposite and antibody for the detection of patulin. Food Chem. 342 https://doi.org/10.1016/j.foodchem.2020.128257.

Sotnikov, D.V., Berlina, A.N., Ivanov, V.S., Zherdev, A.V., Dzantiev, B.B., 2019. Adsorption of proteins on gold nanoparticles: one or more layers? Colloids Surf. B Biointerfaces 173, 557–563. https://doi.org/10.1016/j.colsurfb.2018.10.025.

Steen Redeker, E., Ta, D.T., Cortens, D., Billen, B., Guedens, W., Adriaensens, P., 2013. Protein engineering for directed immobilization. Bioconjugate Chem. 24, 1761–1777. https://doi.org/10.1021/bc4002823.

Sylvestre, J.P., Poulin, S., Kabashin, A.V., Sacher, E., Meunier, M., Luong, J.H.T., 2004. Surface chemistry of gold nanoparticles produced by laser ablation in aqueous media. J. Phys. Chem. B 108, 16864–16869. https://doi.org/10.1021/jp047134+.

Tai, M.J.Y., Perumal, V., Gopinath, S.C.B., Raja, P.B., Ibrahim, M.N.M., Jantan, I.N., Suhaimi, N.S.H., Liu, W.W., 2021. Laser-scribed graphene nanofiber decorated with oil palm lignin capped silver nanoparticles: a green biosensor. Sci. Rep. 11 https://doi.org/10.1038/s41598-021-85039-2.

Thakur, P.S., Sankar, M., 2022. Nanobiosensors for biomedical, environmental, and food monitoring applications. Mater. Lett. 311, 131540 https://doi.org/10.1016/j.matlet.2021.131540.

Thomsen, M., Skovlund, E., Sorbye, H., Bolstad, N., Nustad, K.J., Glimelius, B., Pfeiffer, P., Kure, E.H., Johansen, J.S., Tveit, K.M., Christoffersen, T., Guren, T.K., 2018. Prognostic role of carcinoembryonic antigen and carbohydrate antigen 19-9 in metastatic colorectal cancer: a BRAF-mutant subset with high CA 19-9 level and poor outcome. Br. J. Cancer 118 (12 118), 1609–1616. https://doi.org/10.1038/s41416-018-0115-9, 2018.

Torrente-Rodríguez, R.M., Lukas, H., Tu, J., Min, J., Yang, Y., Xu, C., Rossiter, H.B., Gao, W., 2020. SARS-CoV-2 RapidPlex: a graphene-based multiplexed telemedicine platform for rapid and low-cost COVID-19 diagnosis and monitoring. Matter 3, 1981–1998. https://doi.org/10.1016/j.matt.2020.09.027.

Tu, J., Min, J., Song, Y., Xu, C., Li, J., Moore, J., Hanson, J., Hu, E., Parimon, T., Wang, T. Y., Davoodi, E., Chou, T.F., Chen, P., Hsu, J.J., Rossiter, H.B., Gao, W., 2023. A wireless patch for the monitoring of C-reactive protein in sweat. Nat. Biomed. Eng. 2023, 1–14. https://doi.org/10.1038/s41551-023-01059-5.

Wan, Z., Umer, M., Lobino, M., Thiel, D., Nguyen, N.T., Trinchi, A., Shiddiky, M.J.A., Gao, Y., Li, Q., 2020. Laser induced self-N-doped porous graphene as an electrochemical biosensor for femtomolar miRNA detection. Carbon N Y 163, 385–394. https://doi.org/10.1016/j.carbon.2020.03.043.

Wang, A., Vangala, K., Vo, T., Zhang, D., Fitzkee, N.C., 2014. A three-step model for protein-gold nanoparticle adsorption. J. Phys. Chem. C 118, 8134–8142. https://doi.org/10.1021/jp411543y.

Wang, G., Chen, J., Huang, L., Chen, Y., Li, Y., 2021. A laser-induced graphene electrochemical immunosensor for label-free CEA monitoring in serum. Analyst 146, 6631–6642. https://doi.org/10.1039/D1AN01011E.

Wang, J., Dong, X., Xu, R., Li, S., Chen, P., Chan-Park, M.B., 2012. Template-free synthesis of large anisotropic gold nanostructures on reduced graphene oxide. Nanoscale 4, 3055–3059. https://doi.org/10.1039/C2NR30465A.

Wang, Y., Li, Y., Liu, C., Dong, N., Liu, D., You, T., 2023. Laser induced graphene electrochemical aptasensor based on tetrahedral DNA for ultrasensitive on-site detection of microcystin-LR. Biosens. Bioelectron. 239 https://doi.org/10.1016/j.bios.2023.115610.

Xia, J., Chen, F., Li, J., Tao, N., 2009. Measurement of the quantum capacitance of graphene, 2009 Nat. Nanotechnol. 4 (8 4), 505–509. https://doi.org/10.1038/nnano.2009.177.

Ye, R., Peng, Z., Wang, T., Xu, Y., Zhang, J., Li, Y., Nilewski, L.G., Lin, J., Tour, J.M., 2015. In situ formation of metal oxide nanocrystals embedded in laser-induced graphene. ACS Nano 9, 9244–9251. https://doi.org/10.1021/acsnano.5b04138.

You, Z., Qiu, Q., Chen, H., Feng, Y., Wang, X., Wang, Y., Ying, Y., 2020. Laser-induced noble metal nanoparticle-graphene composites enabled flexible biosensor for pathogen detection. Biosens. Bioelectron. 150, 111896 https://doi.org/10.1016/j.bios.2019.111896.

Zhan, C., Neal, J., Wu, J., Jiang, D.E., 2015. Quantum effects on the capacitance of graphene-based electrodes. J. Phys. Chem. C 119, 22297–22303. https://doi.org/10.1021/acs.jpcc.5b05930.

Zhang, H., Yang, D., Lau, A., Ma, T., Lin, H., Jia, B., 2021. Hybridized graphene for supercapacitors: beyond the limitation of pure graphene. Small 17, 2007311. https://doi.org/10.1002/smll.202007311.

Zhang, J., Zhu, J., Chao, J., 2023. Recent advances in DNA-based electrogenerated chemiluminescence biosensors. Sensors and Diagnostics. https://doi.org/10.1039/d3sd00027c.

Zhao, G., Zhu, H., 2020. Cation–π interactions in graphene-containing systems for water treatment and beyond. Adv. Mater. 32, 1905756 https://doi.org/10.1002/adma.201905756.

Zhao, L., Rosati, G., Piper, A., de Carvalho Castro e Silva, C., Hu, L., Yang, Q., Della Pelle, F., Alvarez-Diduk, R.R., Merkoçi, A., 2023. Laser reduced graphene oxide electrode for pathogenic Escherichia coli detection. ACS Appl. Mater. Interfaces 15, 9033. https://doi.org/10.1021/acsami.2c20859.

Zhu, C., Yang, G., Li, H., Du, D., Lin, Y., 2014. Electrochemical sensors and biosensors based on nanomaterials and nanostructures. Anal. Chem. 87, 230–249. https://doi.org/10.1021/ac5039863.